



ELSEVIER

Contents lists available at ScienceDirect

Comptes Rendus Mecanique

www.sciencedirect.com



Frontiers of micro and nanomechanics of materials: Soft or amorphous matter, surface effects

Micropolar modeling of planar orthotropic rectangular chiral lattices



Yi Chen, Xiaoning Liu*, Gengkai Hu**

Key Laboratory of Dynamics and Control of Flight Vehicle, Ministry of Education, School of Aerospace Engineering, Beijing Institute of Technology, Beijing 100081, China

ARTICLE INFO

Article history:

Received 4 May 2013

Accepted 11 November 2013

Available online 20 May 2014

Keywords:

Chiral micropolar elasticity

Orthotropic

Rectangular chiral lattice

Two-dimensional

ABSTRACT

Rectangular chiral lattices possess a two-fold symmetry; in order to characterize the overall behavior of such lattices, a two-dimensional orthotropic chiral micropolar theory is proposed. Eight additional material constants are necessary to represent the anisotropy in comparison with triangular ones, four of which are devoted to chirality. Homogenization procedures are also developed for the chiral lattice with rigid or deformable circles, all material constants in the developed micropolar theory are derived analytically for the case of the rigid circles and numerically for the case of the deformable circles. The dependences of these material constants and of wave propagation on the microstructural parameters are also examined.

© 2014 Published by Elsevier Masson SAS on behalf of Académie des sciences.

1. Introduction

Lattice materials are promising in a variety of engineering applications due to their high stiffness-to-weight ratio and designable features [1]. Lattice structures of various topologies have been proposed and extensively investigated. An interesting class of lattices is the one that exhibits negative Poisson ratios, namely auxetic lattice materials, and may find many potential applications [2,3]. A well-known example of the auxetic lattice is a triangular chiral lattice proposed by Prall and Lakes [4]. Its geometric pattern and behavior are controlled by a single continuously varying topological parameter, and its unique property has been examined by many researchers under both static [5,6] and dynamic [7] loading conditions with a number of targeted applications. The chiral lattices with other topologies, e.g. square chiral lattices, hexagonal chiral lattices, are also investigated [5,6].

Non-chiral lattices are usually homogenized as a non-chiral micropolar continuum in order to characterize the related size-dependent behaviors [8,9]. Although classical Cauchy elasticity theory [4,6] and non-chiral micropolar theory [10] as well as still utilized to model the auxetic behavior of planar chiral lattice structures, few works are devoted to the characterization of the chiral nature of the lattices. Actually, it is well known that the classical elasticity cannot admit chirality [11]. Therefore, in order to model the chiral lattice, a generalized continuum theory or a higher-order model has to be utilized.

There are different higher-order continuum theories which can take into account the chiral nature of the materials. For strain gradient theory, Auffray et al. [12,13] explained the elastic tensors in two-dimensional (2D) and three-dimensional (3D) cases for all material symmetry groups, including chiral ones. Since an up-to-6th order elastic tensor is introduced in

* Corresponding author. Tel.: +86 10 68912735.

** Corresponding author. Tel.: +86 10 68918363.

E-mail addresses: liuxn@bit.edu.cn (X. Liu), hugeng@bit.edu.cn (G. Hu).

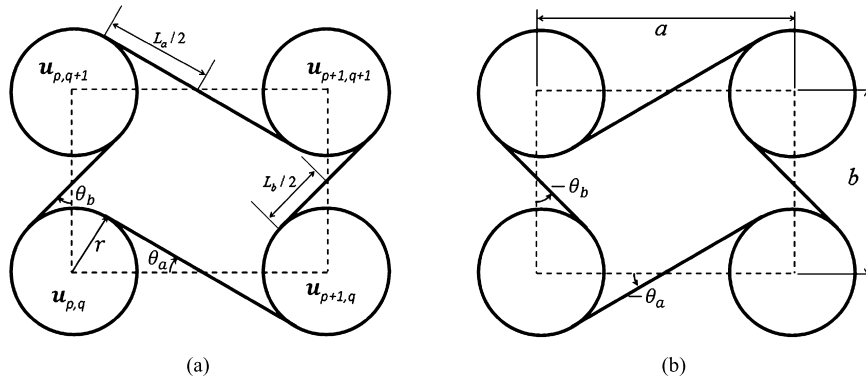


Fig. 1. Geometry of the rectangular chiral lattice, shown with (a) $\theta_a, \theta_b > 0$ and (b) its reversion $\theta_a, \theta_b < 0$.

strain gradient theory, it can capture more information, including the compressibility of the microstructure. However, as in the following, the most pronounced feature of 2D chiral materials investigated in this paper is the coupling between local rotation and bulk deformation, which is the origin of many unusual behaviors (negative Poisson’s ratio, high compressibility, etc.) of such materials. To this end, micropolar theory [14,15] is more intuitive and has been adopted to model the 2D chiral lattices. The 3D isotropic chiral materials (also called hemitropic) are mostly investigated [11,16,17], where three additional material constants compared to the non-chiral theory are introduced. The chiral parameters change their signs according to the handedness of the microstructure. The developed theory provides an efficient tool to model chiral effect of materials and structures, e.g., nanotubes [18,19], mechanics of bone [20], and wave propagation in chiral solids [21]. However, it was found that 3D chiral micropolar theory cannot be applied to a 2D chiral lattice material. To remedy this problem, recently Liu et al. [22] proposed a micropolar model for a 2D isotropic chiral solid, based on which the triangular chiral lattice is modeled from. It was found that the 2D chiral micropolar model is completely different from that of the 3D case either in the mathematical form or in the physical presentation. The unique mechanism of coupling between bulk deformation and particle rotation is demonstrated for 2D chiral solids. Furthermore, the micropolar constitutive equation for 2D orthotropic chiral solids is also established with the help of the theory of irreducible orthogonal decomposition of tensors; the effective material constants are derived for a square lattice with rigid circles [23].

In this paper, a more general rectangular chiral lattice will be considered, and both cases of rigid and deformable circles will be taken into account. The influence of deformable circles will be examined and the dependence of the effective properties on the microstructure, the auxetic behavior as well as the wave propagation of the rectangular chiral lattice will also be investigated. The manuscript is organized as follows. Following a description of the geometric properties of the rectangular chiral lattice in Section 2, a homogenization procedure is developed for both cases of rigid and deformable circles, respectively in Section 3. In Section 4, the theory is illustrated by examining the dependence of the effective material constants and of plane wave propagation on microstructure. The main results of this work are summarized in Section 5.

2. Geometry of a rectangular chiral lattice

The geometry of the considered rectangular chiral lattice is depicted in Fig. 1, which consists of circles of radius r arranged in a rectangular array with the horizontal and vertical lattice constants a and b , respectively. The circles are linked by straight ligaments of lengths L_a and L_b along the two directions, and the ligaments are required to be tangential to the circles. A unit cell with the area $A_{cell} = ab$ is highlighted by the dashed line. The angle between the line connecting the horizontal circle centers and the horizontal ligament is denoted by θ_a . Accordingly, in the vertical direction, a similar angle parameter θ_b can also be defined. Only three of these geometric parameters are independent and the following relations hold:

$$2r = a \sin \theta_a = b \sin \theta_b, \quad L_a = a \cos \theta_a, \quad L_b = b \cos \theta_b \tag{1}$$

When $a < b$, θ_a can be within the $[-\pi/2, \pi/2]$ range, while the value of θ_b can only vary within the $[-\arcsin(a/b), \arcsin(a/b)]$ range, since in the limiting case when $\theta_a = \pm\pi/2$, the horizontal ligaments vanish and the circles touch each other horizontally. θ_a and θ_b are denoted as topology parameters due to their important role on the layout and the mechanical behavior of the lattice [4,10]. With the variation of these angles, the lattice configuration changes dramatically from a traditional rectangle lattice to packed circles, as shown in Fig. 2. The variations of θ_a and θ_b also monitor the transition from a bending dominated to an axially dominated behavior. As shown in Fig. 1, we also adopt a sign convention for θ_a and θ_b depending on the relative orientation of the ligament and the link of circle centers. The reverse of the sign of these angles implies that the lattice is mirror reflected, or equivalently that its handedness is reversed. This operation cannot be achieved by an in-plane rotation due to its chiral nature. When $\theta_a = \theta_b = 0$ the circles shrink to dots and chirality disappears from the lattice.

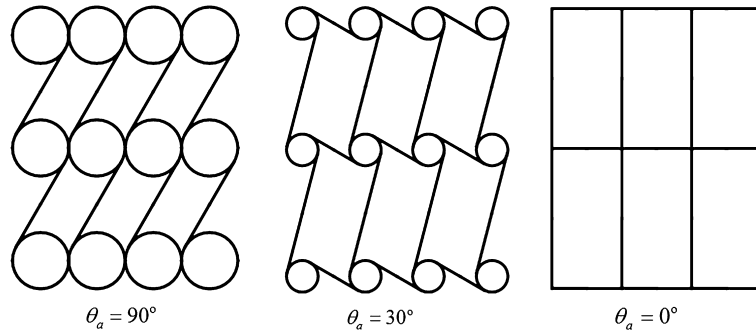


Fig. 2. Lattice configurations corresponding to different topology parameters.

The wall thicknesses of the ligaments and the circle are assumed to be the same as t . Further, for convenience, a dimensionless parameter $\eta = t/a$ is defined, which indicates the slenderness of the lattice walls. The Young modulus of the underlying lattice material is denoted in the following by E_s .

3. Micropolar modeling

In this section, the planar rectangular chiral lattice will be homogenized as a 2D micropolar medium. Therefore basic ingredients of the 2D orthotropic chiral micropolar theory will be briefly recalled, and then the homogenizations of the lattices with rigid circles and deformable circles are performed, respectively, to derive the effective constants in the 2D orthotropic chiral micropolar theory.

3.1. Orthotropic chiral micropolar constitutive model

Micropolar theory endows every material point with three rotational degrees of freedom ϕ_i in addition to displacements u_i [15]. For a 2D micropolar problem defined in the x_1 - x_2 plane, it is required that $u_3 = \phi_1 = \phi_2 = \partial/\partial x_3 = 0$, and the geometric and equilibrium equations of micropolar elasticity are reduced to:

$$\varepsilon_{ij} = u_{j,i} + e_{ji}\phi, \quad k_i = \phi_{,i} \tag{2a}$$

$$\sigma_{ji,j} = \rho \partial^2 u_i / \partial t^2, \quad m_{i,i} + e_{ij}\sigma_{ij} = j \partial^2 \phi / \partial t^2 \tag{2b}$$

where $\phi \equiv \phi_3$ is the out of plane micro-rotation, ε_{ij} and σ_{ij} are respectively the non-symmetric strain and stress, $k_i \equiv k_{i3}$ and $m_i \equiv m_{i3}$ are respectively the reduced curvature and couple stress, ρ and j are separately the density and micro-inertia, $e_{ij} \equiv e_{3ij}$ can be considered as a 2D Levi-Civita tensor, and the Einstein summation convention is used. Here and after, the subscripts range from 1 to 2. For a general 2D micropolar medium, the constitutive equations are reduced to the following form:

$$\sigma_{ij} = C_{ijkl}\varepsilon_{kl} + B_{ijk}k_k, \quad m_k = B_{ijk}\varepsilon_{ij} + D_{kl}k_l \tag{3}$$

where C_{ijkl} is the elastic tensor of rank four, D_{kl} is the higher order elastic tensor of rank two, and B_{ijk} is the cross elastic tensor relating the ordinary and higher-order quantities. The density of strain energy reads:

$$w = \frac{1}{2} C_{ijkl}\varepsilon_{ij}\varepsilon_{kl} + \frac{1}{2} D_{ij}k_i k_j + \varepsilon_{ij} B_{ijk}k_k \tag{4}$$

Note that a medium is called non-centrosymmetric when $\mathbf{B} \neq 0$, and in 3D case the \mathbf{B} tensor contains the information of chirality [11]. However, it has been proved that for a 2D (chiral) isotropic and orthotropic micropolar medium, the \mathbf{B} tensor must be zero, hence the chiral behavior can only be characterized through the \mathbf{C} and \mathbf{D} tensors [23]. The constitutive relation for a general 2D orthotropic chiral micropolar medium has recently been established by using the theory of irreducible orthogonal decomposition of tensors [23], and it is summarized here for completeness. Adopting the following Voigt form of the strain and strain:

$$\begin{aligned} \boldsymbol{\sigma} &= (\sigma_{11} \quad \sigma_{22} \quad \sigma_{12} \quad \sigma_{21})^T, & \boldsymbol{\varepsilon} &= (\varepsilon_{11} \quad \varepsilon_{22} \quad \varepsilon_{12} \quad \varepsilon_{21})^T \\ \mathbf{m} &= (m_1 \quad m_2)^T, & \mathbf{k} &= (k_1 \quad k_2)^T \end{aligned} \tag{5}$$

the 2D orthotropic chiral micropolar constitutive relation can be expressed in a matrix form as:

$$\boldsymbol{\sigma} = \mathbf{C}\boldsymbol{\varepsilon}, \quad \mathbf{m} = \mathbf{D}\mathbf{k} \tag{6}$$

The constitutive matrices **C** and **D** possess a hierarchical structure and can be decomposed into several parts according to the symmetry of the underlying microstructure as

$$\begin{aligned} \mathbf{C} &= \mathbf{C}^{\text{hemi}} + \mathbf{C}^{\text{4-fold}} + \mathbf{C}^{\text{2-fold}} \\ \mathbf{D} &= \mathbf{D}^{\text{hemi}} + \mathbf{D}^{\text{2-fold}} \end{aligned} \tag{7}$$

where each individual part reads:

$$\mathbf{C}^{\text{hemi}} = \begin{pmatrix} \lambda + 2\mu & \lambda & A & -A \\ \lambda & \lambda + 2\mu & A & -A \\ A & A & \mu + \kappa & \mu - \kappa \\ -A & -A & \mu - \kappa & \mu + \kappa \end{pmatrix} \tag{8a}$$

$$\mathbf{C}^{\text{4-fold}} = \begin{pmatrix} \alpha & -\alpha & B & B \\ -\alpha & \alpha & -B & -B \\ B & -B & -\alpha & -\alpha \\ B & -B & -\alpha & -\alpha \end{pmatrix} \tag{8b}$$

$$\mathbf{C}^{\text{2-fold}} = \begin{pmatrix} \beta_1 + \beta_2 & 0 & C_1 & C_2 \\ 0 & -(\beta_1 + \beta_2) & C_2 & C_1 \\ C_1 & C_2 & \beta_1 - \beta_2 & 0 \\ C_2 & C_1 & 0 & -(\beta_1 - \beta_2) \end{pmatrix} \tag{8c}$$

$$\mathbf{D}^{\text{hemi}} = \begin{pmatrix} \gamma & 0 \\ 0 & \gamma \end{pmatrix} \tag{9a}$$

$$\mathbf{D}^{\text{2-fold}} = \begin{pmatrix} \gamma_1 & \gamma_2 \\ \gamma_2 & -\gamma_1 \end{pmatrix} \tag{9b}$$

respectively. If the material is hemitropic (isotropic chiral), e.g., for a triangular or a hexagonal chiral lattice, only \mathbf{C}^{hemi} and \mathbf{D}^{hemi} are kept in Eq. (7). According to Eqs. (8a) and (9a), besides the traditional isotropic micropolar material constants λ, μ, κ and γ , a chiral parameter A is introduced. The chiral parameter will reverse its sign when the handedness of the material is reversed. If the material possesses 4-fold symmetry, taking the square chiral lattice as an example, $\mathbf{C}^{\text{4-fold}}$ should be *additionally* included into the **C** matrix. Regarding Eq. (8b), besides the hemitropic constants, two additional constants α and B are introduced, and B is the chiral parameter. If the material possesses 2-fold symmetry, as a rectangular chiral lattice for example, $\mathbf{C}^{\text{2-fold}}$ and $\mathbf{D}^{\text{2-fold}}$ should further be taken into account. Regarding Eqs. (8c) and (9b), six additional material constants $\beta_1, \beta_2, C_1, C_2, \gamma_1$ and γ_2 are introduced, where C_1, C_2 and γ_2 are chiral parameters.

By using such decomposition, the transformation of the constitutive matrix can be easily calculated under any direction. Assuming that the coordinate system rotates θ , the constants of 4-fold symmetry are transformed by

$$\begin{pmatrix} \alpha' \\ B' \end{pmatrix} = \begin{pmatrix} \cos 4\theta & \sin 4\theta \\ -\sin 4\theta & \cos 4\theta \end{pmatrix} \begin{pmatrix} \alpha \\ B \end{pmatrix} \tag{10}$$

while the constants of 2-fold symmetry are transformed by

$$\begin{pmatrix} \beta_2' \\ C_1' \end{pmatrix} = \begin{pmatrix} \cos 2\theta & \sin 2\theta \\ -\sin 2\theta & \cos 2\theta \end{pmatrix} \begin{pmatrix} \beta_2 \\ C_1 \end{pmatrix} \tag{11a}$$

$$\begin{pmatrix} \beta_1' \\ C_2' \end{pmatrix} = \begin{pmatrix} \cos 2\theta & \sin 2\theta \\ -\sin 2\theta & \cos 2\theta \end{pmatrix} \begin{pmatrix} \beta_1 \\ C_2 \end{pmatrix} \tag{11b}$$

$$\begin{pmatrix} \gamma_1' \\ \gamma_2' \end{pmatrix} = \begin{pmatrix} \cos 2\theta & \sin 2\theta \\ -\sin 2\theta & \cos 2\theta \end{pmatrix} \begin{pmatrix} \gamma_1 \\ \gamma_2 \end{pmatrix} \tag{11c}$$

The hemitropic material constants remain unchanged.

3.2. Homogenization of the lattice with rigid circles

To formulate the homogenization procedure analytically, the circles of the chiral lattice are assumed in this subsection to be rigid. Let vector $\mathbf{u}_i = \{u_i \ v_i \ \phi_i\}^T$ denote the displacement and rotation DOFs of the center of the rigid circle i . The rigid circle imposes a constraint on the motion of the ends of deformable ligaments $\tilde{\mathbf{u}}_i = \{\tilde{u}_i \ \tilde{v}_i \ \tilde{\phi}_i\}^T$, which relates \mathbf{u}_i by $\tilde{\mathbf{u}}_i = \mathbf{T}(\Theta_i)\mathbf{u}_i$ with the transformation matrix being

$$\mathbf{T}(\Theta_i) = \begin{pmatrix} 1 & 0 & -r \sin \Theta_i \\ 0 & 1 & r \cos \Theta_i \\ 0 & 0 & 1 \end{pmatrix} \tag{12}$$

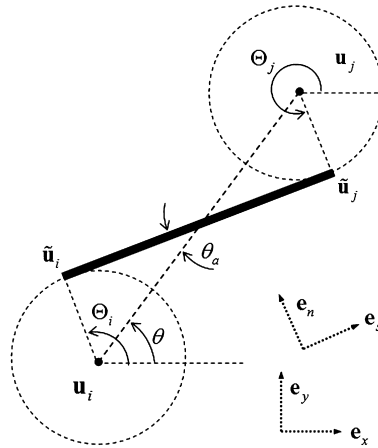


Fig. 3. Geometry and symbol definitions for the analysis of a single ligament.

where Θ_i is the azimuthal angle of the beam end on the circle i (see Fig. 3). The relations $\Theta_i = \pi/2 + \theta - \theta_a$ and $\Theta_j = 3\pi/2 + \theta - \theta_a$, giving the topological parameter θ_a and the direction angle θ of the circles i and j linked by the beam, are implied. The DOFs of the beam ends $\tilde{\mathbf{u}}'$ in the local system (\mathbf{e}_s – \mathbf{e}_n in Fig. 3) are then linked to the DOFs $\mathbf{u} = \{\mathbf{u}_i \ \mathbf{u}_j\}^T$ at the circle centers as $\tilde{\mathbf{u}}' = \mathbf{R}(\theta)\mathbf{T}(\Theta_1, \Theta_2)\mathbf{u}$, where

$$\mathbf{T}(\Theta_1, \Theta_2) = \begin{pmatrix} \mathbf{T}(\Theta_1) & \mathbf{0} \\ \mathbf{0} & \mathbf{T}(\Theta_2) \end{pmatrix} \tag{13}$$

$$\mathbf{R}(\theta) = \begin{pmatrix} \mathbf{R}_{3 \times 3}(\theta) & \mathbf{0} \\ \mathbf{0} & \mathbf{R}_{3 \times 3}(\theta) \end{pmatrix} \tag{14}$$

$$\mathbf{R}_{3 \times 3}(\theta) = \begin{pmatrix} \cos(\theta - \theta_a) & \sin(\theta - \theta_a) & 0 \\ -\sin(\theta - \theta_a) & \cos(\theta - \theta_a) & 0 \\ 0 & 0 & 1 \end{pmatrix} \tag{15}$$

With the help of the Euler–Bernoulli beam theory, the stiffness matrix of the ligaments in its local system is expressed as

$$\mathbf{K}' = \frac{E_s t}{6L} \begin{pmatrix} 1 & 0 & 0 & -1 & 0 & 0 \\ & 6t^2/L^2 & 3t^2/L & 0 & -6t^2/L^2 & 3t^2/L \\ & & 2t^2 & 0 & -3t^2/L & t^2 \\ & & & 1 & 0 & 0 \\ & sym & & & 6t^2/L^2 & -3t^2/L \\ & & & & & 2t^2 \end{pmatrix} \tag{16}$$

where L is the beam length. In the global system, the stiffness matrix of a single ligament is obtained as

$$\mathbf{K} = \mathbf{T}^T(\Theta_i, \Theta_j)\mathbf{R}^T(\theta)\mathbf{K}'\mathbf{R}(\theta)\mathbf{T}(\Theta_i, \Theta_j) \tag{17}$$

Referring to Fig. 1a, the strain energies of the two ligaments in a unit cell can be expressed by

$$\begin{aligned} w_1 &= \frac{1}{2} \{\mathbf{u}_{p,q} \ \mathbf{u}_{p+1,q}\}^T \mathbf{K}|_{\theta=0, L=L_a} \{\mathbf{u}_{p,q} \ \mathbf{u}_{p+1,q}\} \\ w_2 &= \frac{1}{2} \{\mathbf{u}_{p,q} \ \mathbf{u}_{p,q+1}\}^T \mathbf{K}|_{\theta=\pi/2, L=L_b} \{\mathbf{u}_{p,q} \ \mathbf{u}_{p,q+1}\} \end{aligned} \tag{18}$$

respectively, and therefore the density of the deformation energy of the lattice reads

$$w_{p,q}^{\text{cell}} = (w_1 + w_2)/A_{\text{cell}} \tag{19}$$

In order to express the energy density in terms of strains and curvatures, the following expansions are made based on the Taylor series:

$$\begin{aligned} u_{p+1,q} &= u_{p,q} + \varepsilon_{11} \Delta x, & u_{p,q+1} &= u_{p,q} + (\varepsilon_{21} - \phi) \Delta y \\ v_{p+1,q} &= v_{p,q} + (\varepsilon_{12} + \phi) \Delta x, & v_{p,q+1} &= v_{p,q} + \varepsilon_{22} \Delta y \\ \phi_{p+1,q} &= \phi_{p,q} + k_1 \Delta x, & \phi_{p,q+1} &= \phi_{p,q} + k_2 \Delta y \end{aligned} \tag{20}$$

where $\Delta x = a$, $\Delta y = b$, and the terms of higher order $O(\Delta x^2, \Delta y^2)$ are ignored. The micropolar elastic tensors are then obtained from:

$$C_{ijkl} = \frac{\partial^2 w}{\partial \varepsilon_{ij} \partial \varepsilon_{kl}}, \quad D_{ij} = \frac{\partial^2 w}{\partial k_i \partial k_j} \quad (21)$$

Finally, the homogenized material constants of rectangular chiral lattices are obtained and expressed in the principal direction of the lattices as follows.

Hemitropic:

$$\begin{aligned} \lambda &= \frac{E_s \eta}{8} \left[2(\cot 2\theta_b + \cot 2\theta_a) - \frac{\eta^2}{\sin^2 \theta_a} (\tan \theta_a + \tan \theta_b - \tan^3 \theta_a - \tan^3 \theta_b) \right] \sin \theta_b \\ \mu &= \frac{E_s \eta}{4} \left[\left(1 + \frac{\sin 2\theta_a}{\sin 2\theta_b} \right) + \eta^2 \frac{1}{\cos^2 \theta_a} \left(1 + \frac{\sin \theta_b \cos^3 \theta_a}{\sin \theta_a \cos^3 \theta_b} \right) \right] \frac{\sin \theta_b}{\sin 2\theta_a} \\ \kappa &= \frac{E_s \eta \tan \theta_b \sin(\theta_b + \theta_a) (\sin^2 \theta_a + \eta^2)}{2 \sin 2\theta_a \sin \theta_a} \\ A &= \frac{E_s \eta}{4} [\eta^2 (\tan^2 \theta_b + \tan^2 \theta_a) - 2 \sin^2 \theta_a] \frac{\sin \theta_b}{\sin^2 \theta_a} \\ \gamma &= \frac{E_s \eta a^2 (\sin 2\theta_b + \sin 2\theta_a) (4\eta^2 - 3 \sin^2 \theta_a)}{24 \cos \theta_b \sin 2\theta_a} \end{aligned} \quad (22)$$

4-fold symmetry:

$$\begin{aligned} \alpha &= \lambda \\ B &= A \end{aligned} \quad (23)$$

2-fold symmetry:

$$\begin{aligned} \beta_1 &= \frac{E_s \eta}{4} \left[\eta^2 \left(\frac{\tan \theta_a}{\cos^2 \theta_a} - \frac{\tan \theta_b}{\cos^2 \theta_b} \right) + 2 \sin^2 \theta_a \left(\frac{1}{\sin 2\theta_a} - \frac{1}{\sin 2\theta_b} \right) \right] \frac{\sin \theta_b}{\sin^2 \theta_a} \\ \beta_2 &= \frac{E_s \eta}{2} \left[\frac{\eta^2 (\tan^2 \theta_b \cot 2\theta_b - \tan^2 \theta_a \cot 2\theta_a)}{\sin^2 \theta_a} + (\cot 2\theta_a - \cot 2\theta_b) \right] \sin \theta_b \\ C_1 &= E_s \eta^3 \frac{\tan \theta_b (\cos 2\theta_b - \cos 2\theta_a)}{\cos \theta_b \sin^2 2\theta_a} \\ C_2 &= 0 \\ \gamma_1 &= \frac{E_s \eta a^2 (\sin 2\theta_b - \sin 2\theta_a) (4\eta^2 - 3 \sin^2 \theta_a)}{24 \sin 2\theta_a \cos \theta_b} \\ \gamma_2 &= 0 \end{aligned} \quad (24)$$

From Eqs. (22)–(24), it is easy to verify that the chiral material constants A , B and C_1 change their signs when the topology parameters θ_a and θ_b change the signs simultaneously, i.e., the handedness of the lattice is reversed, while the other non-chiral parameters remain unchanged. For the case of $\theta_a = \theta_b$, i.e., for the square lattice, all 2-fold symmetry constants vanish. It is worth to note that Eq. (23) holds only in the principal coordinate system as that in Fig. 1. In the other coordinate system, α and B vary according to Eq. (10). Finally, when $\theta_a = \theta_b = 0$, the lattice reduces to a non-chiral traditional rectangular lattice with the same micropolar constants as those given by Kumar and Christensen [9].

3.3. Deformable circles

When the circles are deformable, analytical expressions of the effective constants are difficult to obtain, since many straight beam segments or curved beams are necessary to model the deformable circles. Instead, a numerical procedure based on the finite-element calculation of the single unit cell is employed in this section. The analyzed unit cell model is shown in Fig. 4, where the node numbering and the DOFs at the cell boundary are depicted.

Unlike the rigid circle, the motion of a deformable circle is not easy to define by three overall DOFs (u, v, ϕ). To this end, the method of force-distributed constraint equations is employed. A virtual node is created at the center of the circle, whose DOFs (called master) is related to the DOFs (called slave) of all the nodes on the deformable circle by the constraint equations [22]. This approach allows one to specify the motion of the deformable circle in an overall average sense by prescribing the DOFs of the virtual node at the circle center.

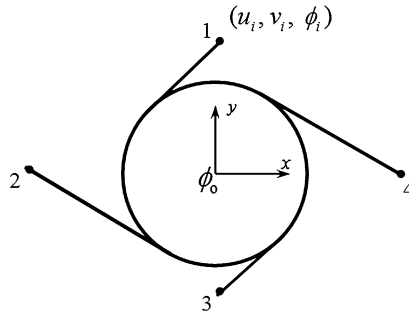


Fig. 4. Finite element model of the unit cell employed to the lattice with deformable circles.

Table 1

Prescribed DOFs corresponding to independent strain states.

	$\varepsilon_{11} = 1$	$\varepsilon_{22} = 1$	$\varepsilon_{12} = 1$	$\varepsilon_{21} = 1$	$\phi_{,1} = 1$	$\phi_{,2} = 1$
u_i	x_i	0	$y_i/2$	$y_i/2$	Periodic	Periodic
v_i	0	y_i	$x_i/2$	$x_i/2$	Periodic	Periodic
ϕ_i	Periodic	Periodic	Periodic	Periodic	x_i	y_i
ϕ_0	0	0	$-1/2$	$1/2$	0	0

According to the geometric equation (20) of the micropolar theory, the DOFs at the boundary nodes and central virtual node corresponding to each independent strain state are determined and listed in Table 1, where (x_i, y_i) are the coordinates of the i th node of the unit cell boundary, and the *periodic* means the corresponding DOFs of the node pairs (1, 3) and (2, 4) are coupled.

To numerically determine the effective material constants, a series of linearly independent strain states need to be assumed onto the unit cell model, and then the strain energy density is numerically evaluated. For instance, from Eqs. (4)–(9), the energy density $w = 2\kappa$ corresponds to the strain state $\boldsymbol{\varepsilon} = \{0, 0, -1, 1\}^T$. Other effective constants can be determined in a similar manner.

4. Discussion and numerical results

4.1. Dependence of effective elastic constants on microstructure

First, the dependences of the effective micropolar elastic constants on lattice configurations are examined for rectangular chiral lattices; both rigid circle and deformable circle are considered. In the following, in order to introduce some anisotropy and to focus on the chiral effect, the lattice constants are fixed as $a = 1$ and $b = 2a$, while the size of the circles is dominated by the topology parameter θ_a . It should be noted that θ_b is dependent on θ_a through the relationship: $2 \sin \theta_b = \sin \theta_a$. Accordingly, while the variation range of θ_a is $[-\pi/2, \pi/2]$, the possible value of θ_b is bounded by $[-\pi/6, \pi/6]$.

The ten classical material constants involved in the \mathbf{C} tensor are selectively displayed in Fig. 5 for the rigid circle case as a function of parameter θ_a . Fig. 5a shows the variation of parameters λ and A normalized by E_s . It can be seen that the chiral constant A is an odd function of θ_a and that $|A|$ increases with increasing θ_a in the most part of the region. It should be noted that for the case of the rigid circle, the results of the limiting case $\theta_a \rightarrow 90^\circ$ tend to be infinite and meaningless since the deformable ligaments are vanishingly short. Two cases, $\eta = 1/20$ and $\eta = 1/50$, are compared to show the influence of the beam slenderness ratio. It is shown that the thicker ligaments give a greater chiral constant A , while for λ this dependence is not monotonous. In the principal coordinate system, we have the 4-fold symmetry constants $\alpha = \lambda$ and $B = A$; however they should be transformed according to Eq. (10) when the system rotates. For the constants (μ, κ) shown in Fig. 5b and (β_1, β_2) shown in Fig. 5c, a stiffer behavior is observed for thicker ligaments and larger circles (i.e. larger $|\theta_a|$). The 4-fold symmetry chiral parameter (C_1, C_2) is plotted in Fig. 5d, which shows that C_1 approaches zero within the most part of θ_a region, especially for lattices of thin ligaments. According to Eq. (24), C_2 is always zero for the lattice with the rigid circles.

The effective material constants for the cases of rigid and deformable circles are compared in Fig. 6, where the slenderness ratio is fixed at $\eta = 1/20$. It can be seen that for all the constants, the case of the deformable circles gives very different predictions compared to that in the rigid case. However, when $\theta_a \rightarrow 0$, i.e. the circle tends to vanish, and the two sets of predictions are close. This is understandable since the smaller circle is stiffer with η being fixed. When $|\theta_a|$ becomes larger, a significant discrepancy is observed due to the circle distortion, the dependence of the material constants on θ_a is also more complicated in compared to the rigid case. It is interesting to note from Fig. 6a that although in the principal direction $\alpha = \lambda$ and $B = A$ hold for the rigid circle case, the situation is different if the circles are deformable. Also, it is observed in Fig. 6d that C_2 is no longer zero for the case of the deformable circles.

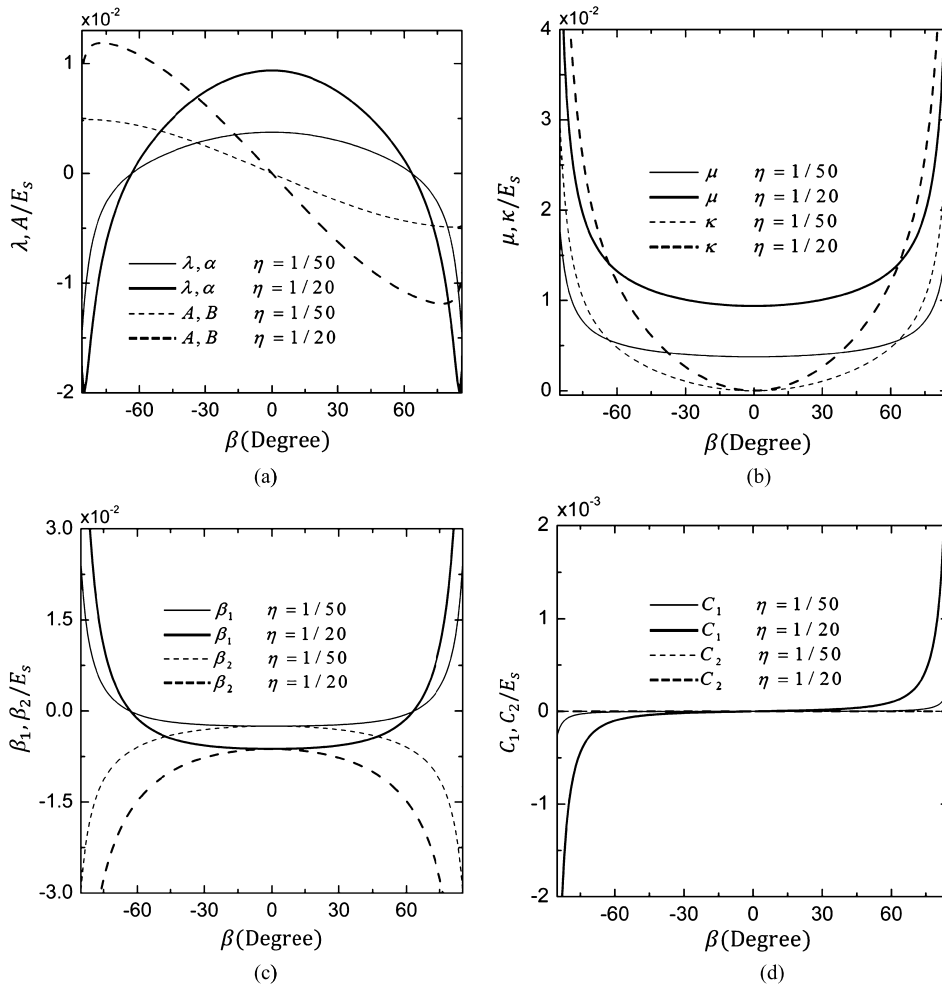


Fig. 5. Variation of effective material constants (a) $\lambda = \alpha$, $A = B$, (b) μ , κ , (c) β_1 , β_2 and (d) C_1 , C_2 in the principal system as a function of θ_a .

It is also interesting to examine the auxetic behavior of the lattice with the proposed model. As shown in Ref. [22], the Young modulus E and Poisson's ratio ν should be redefined regarding the new constitutive relation. Assuming all the stress components except σ_{11} are zero, by using Eqs. (6)–(8) we can express $\nu_0 = -\varepsilon_{22}/\varepsilon_{11}$ and $E_0 = \sigma_{11}/\varepsilon_{11}$ as the predefined material constants, where subscript 0 denotes that stress state along the principal axis x . However, the expressions are quite complicated and not presented here. To obtain the Young's modulus E_θ and the Poisson's ratio ν_θ along an arbitrary direction rotated from x by an angle θ , Eqs. (10) and (11) can be utilized. Fig. 7 displays the variation of E_θ and ν_θ as a function of θ , with $\eta = 1/20$. Two lattice topologies of $\theta_a = 0$ (traditional rectangular lattice) and $\theta_a = 60^\circ$ are compared. For the $\theta_a = 60^\circ$ case, both results for rigid and deformable circles are calculated. For the non-chiral traditional lattice, the Young modulus is much higher in the principal direction, since the ligament tension dominates the deformation, and it drops rapidly in the other direction when the bending modes dominate. However, for the chiral lattice of the $\theta_a = 60^\circ$ case, since the ligament bending can always be induced, the peaks of E_θ are much lower and they do not lie in the principal directions. Roughly the peaks happen in the directions approaching those of the ligaments. It can be proved that for the traditional non-chiral lattice and the chiral lattice with rigid circles, the Poisson ratio is always zero along the principal direction. As shown in Fig. 7b, ν_θ rapidly approaches 1 in the other direction for the traditional rectangular lattice. For the $\theta_a = 60^\circ$ case, ν_θ displays very strong directionality and can only be negative in small ranges of θ , indicating that the auxetic behavior can only happen in a very narrow loading direction range. This is different from the case of triangular chiral lattices. Compared with Fig. 7a, the directions of the negative peaks of ν_θ roughly correspond to the directions of the peaks of E_θ .

4.2. Plane wave propagation

The wave propagation behavior in the rectangular chiral lattice is also examined in this subsection with the proposed model. In an infinite 2D micropolar medium, the plane wave propagating along the $+x$ direction takes the following form:

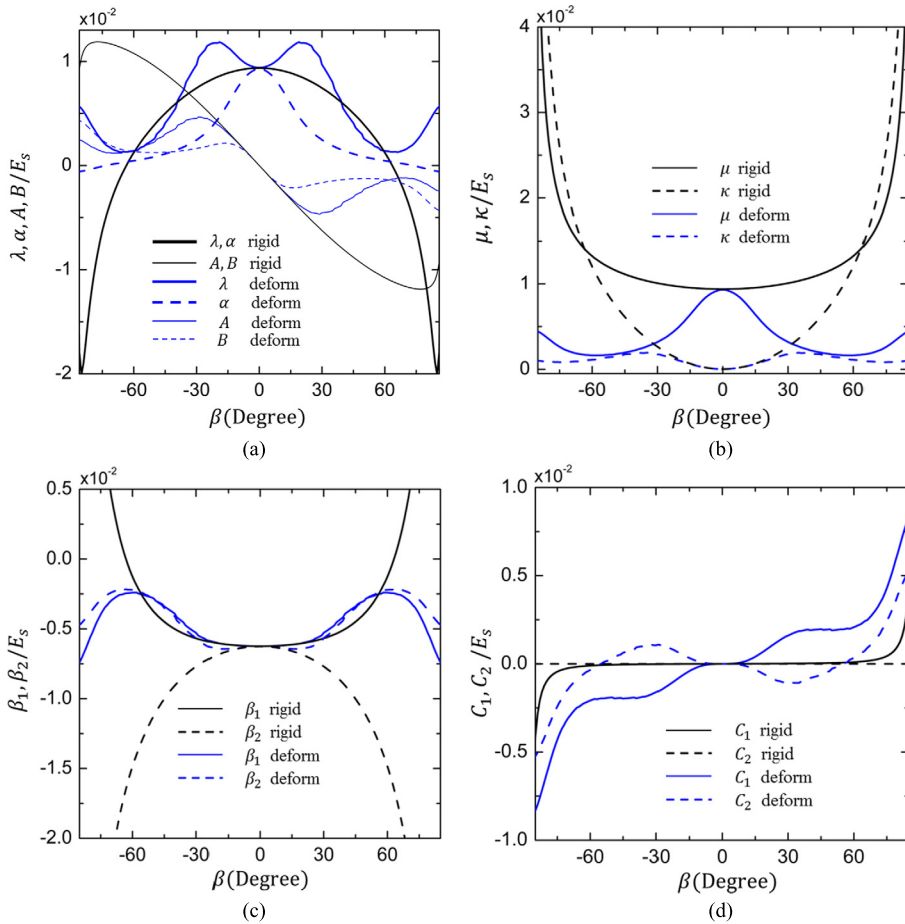


Fig. 6. Comparison of effective material constants (a) λ, α, A, B , (b) μ, κ , (c) β_1, β_2 and (d) C_1, C_2 for the case of rigid and deformable circles.

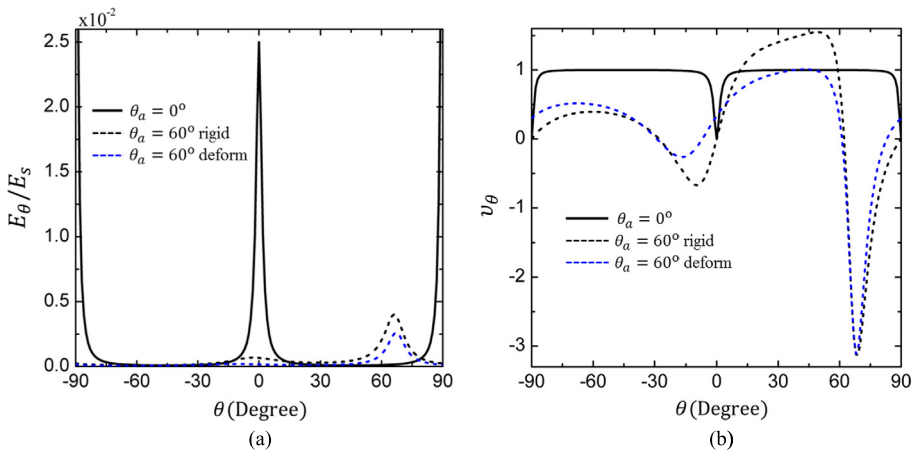


Fig. 7. Variation of effective (a) Young modulus and (b) Poisson's ratio along different directions.

$$(u, v, \phi) = (\hat{u}, \hat{v}, \hat{\phi}) \exp(iq\mathbf{x} - i\omega t) \tag{25}$$

where q and ω denote the wave number and frequency, respectively, $(\hat{u}, \hat{v}, \hat{\phi})$ are the complex amplitudes and $i = \sqrt{-1}$. Substituting Eq. (25) into the dynamical equations of the homogenized media governed by Eqs. (2)–(9), the following secular equation is obtained:

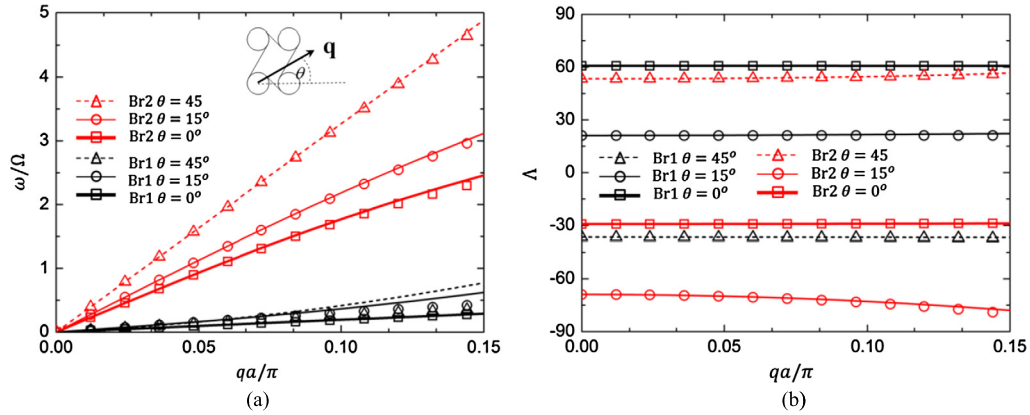


Fig. 8. (a) Dispersion curves and (b) corresponding polarization angle of the first two branches of plane wave propagation along the principal, 15° and 45°, directions, calculated from homogenized (lines) and discrete (dots) models. (For interpretation of the colors in this figure, the reader is referred to the web version of this article.)

$$\begin{pmatrix} (\beta_1 + \beta_2 + \alpha + \lambda + 2\mu)q^2 - \rho\omega^2 & (A + B + C_1)q^2 & (2A + C_1 - C_2)iq \\ (A + B + C_1)q^2 & (\beta_1 - \beta_2 - \alpha + \kappa + \mu)q^2 - \rho\omega^2 & (\beta_1 - \beta_2 + 2\kappa)iq \\ -(2A + C_1 - C_2)iq & -(\beta_1 - \beta_2 + 2\kappa)iq & q^2(\gamma_1 + \gamma_3) + 4\kappa - j\omega^2 \end{pmatrix} \begin{pmatrix} u_0 \\ v_0 \\ \phi_0 \end{pmatrix} = 0 \quad (26)$$

With the help of Eqs. (10) and (11), wave propagation along any direction other than the principal one can be easily analyzed. In the following, Eq. (26) is numerically solved to obtain the dispersion and the wave mode information. Lattices with rigid circles and the corresponding homogenized media are used in the numerical examples. For simplicity, the ligaments are assumed to be massless, and the mass and rotation inertia are lumped to the rigid circles and denoted by m and J , respectively. For the homogenized micropolar media, the effective density $\rho = m/A_{\text{cell}}$ and the micro rotational inertia $j = J/A_{\text{cell}}$ are defined. Lattice parameters $a = 1$, $b = 2$, $\eta = 1/20$ and $m = J = 1$ are fixed in the calculation. For comparison, the exact Bloch wave solutions utilizing the corresponding discrete model are also calculated.

Fig. 8a shows the dispersion curves of the first two branches (in black and red, respectively), whose wave modes are displacement dominated, of the lattice with the topological parameter $\theta_a = 30^\circ$. The third rotational-dominated branch is not shown, since it is similar to that of a traditional micropolar medium. The wave vectors along the $\theta = 0^\circ$ (principal direction), $\theta = 15^\circ$ and $\theta = 45^\circ$ are calculated, respectively. The wave frequency is normalized by $\Omega = 2\sqrt{\eta^3 E_s/m}$. The dispersion curves obtained from the homogenized model agree well with those of the discrete lattice (shown by dots) in the long-wave approximation. Similar to the case of triangular chiral lattices [22], all three branches are coupled together and dispersive, and there is in general no longer pure longitudinal (P) and transverse (S) wave.

Since the particle is always linearly polarized, a polarization angle Λ measured with respect to the wave propagating direction, $\tan \Lambda = \hat{v}/\hat{u}$, is defined to characterize the wave mode shape. In Fig. 8b, the polarization angles corresponding to each dispersive branch in Fig. 8a are plotted as a function of the wave number, where the same line types are used for one-to-one matching. It can be seen that the polarization angle depends on the wave number (and the frequency and wave speed). When the wave propagates in the principal direction, S-dominated ($\Lambda \sim 60^\circ$) and P-dominated ($\Lambda \sim 30^\circ$) waves are observed for the 1st and 2nd branches, and the polarization angles are almost independent of the frequency. In the $\theta = 15^\circ$ and $\theta = 45^\circ$ directions, we have almost the two branches exchanged, i.e., the wave with a lower phase speed is of P-dominated type, and the wave with a higher phase speed is of S-dominated type, and the polarization angles vary with the frequency. This feature is not found for a traditional non-chiral medium.

5. Conclusions

In this work, a rectangular chiral lattice is characterized in the framework of 2D orthotropic chiral micropolar theory. By assuming that the lattice circles are rigid, we derive analytically the expressions of a total of 13 effective micropolar material constants. A numerical homogenization procedure is also developed when the circles of the lattice are deformable. It is shown that the deformability of the circle has a great influence on the mechanical, chiral, and auxetic behavior of the lattice, especially for large deformable circles. The auxetic behavior of rectangular lattices is very different from that of triangular ones; Poisson's ratio can only be negative in a narrow range of loading directions. For plane wave propagation, transition of P- and S-wave modes for the first two branches along different propagating directions is observed. The proposed theory can serve as a valuable tool for modeling and designing rectangular chiral lattice structures.

Acknowledgement

This work was supported in part by National Natural Science Foundation of China under Grants Nos. 11221202, 11290153, 11072031, 11128204, and 11372035.

References

- [1] L.J. Gibson, M.F. Ashby, *Cellular Solids: Structure and Properties*, 2nd ed., Cambridge University Press, Cambridge, 1997.
- [2] R. Lakes, Foam structures with a negative Poisson's ratio, *Science* 235 (1987) 1038–1040.
- [3] K.E. Evans, A. Alderson, Auxetic materials: functional materials and structures from lateral thinking, *Adv. Mater.* 12 (2000) 617–624.
- [4] D. Prall, R.S. Lakes, Properties of a chiral honeycomb with a Poisson's ratio ≈ -1 , *Int. J. Mech. Sci.* 39 (1996) 305–314.
- [5] A. Alderson, K.L. Alderson, D. Attard, K.E. Evans, R. Gatt, J.N. Grima, W. Miller, N. Ravirala, C.W. Smith, K. Zied, Elastic constants of 3-, 4- and 6-connected chiral and anti-chiral honeycombs subject to uniaxial in-plane loading, *Compos. Sci. Technol.* 70 (2010) 1042–1048.
- [6] J. Dirrenberger, S. Forest, D. Jeulin, C. Colin, Homogenization of periodic auxetic materials, *Proc. Eng.* 10 (2011) 1847–1852.
- [7] A. Spadoni, M. Ruzzene, S. Gonella, F. Scarpa, Phononic properties of hexagonal chiral lattices, *Wave Motion* 46 (2009) 435–450.
- [8] J.Y. Chen, Y. Huang, M. Ortiz, Fracture analysis of cellular materials: a strain gradient model, *J. Mech. Phys. Solids* 46 (1998) 789–828.
- [9] R.S. Kumar, D.L. McDowell, Generalized continuum modeling of 2-D periodic cellular solids, *Int. J. Solids Struct.* 41 (2004) 7399–7422.
- [10] A. Spadoni, M. Ruzzene, Elasto-static micropolar behavior of a chiral auxetic lattice, *J. Mech. Phys. Solids* 60 (2012) 156–171.
- [11] R.S. Lakes, R.L. Benedict, Noncentrosymmetry in micropolar elasticity, *Int. J. Eng. Sci.* 20 (1982) 1161–1167.
- [12] N. Auffray, R. Bouchet, Y. Bréchet, Strain gradient elastic homogenization of bi-dimensional cellular media, *Int. J. Solids Struct.* 47 (2010) 1698–1710.
- [13] N. Auffray, H. Le Quang, Q.C. He, Matrix representations for 3D strain-gradient elasticity, *J. Mech. Phys. Solids* 61 (2013) 1202–1223.
- [14] E. Cosserat, F. Cosserat, *Théorie des corps Déformables*, Hermann, Paris, 1909.
- [15] A.C. Eringen, *Microcontinuum Field Theories I: Foundations and Solids*, Springer, New York, 1999.
- [16] R. Lakes, Elastic and viscoelastic behavior of chiral materials, *Int. J. Mech. Sci.* 43 (2001) 1579–1589.
- [17] D. Natroshvili, I.G. Stratis, Mathematical problems of the theory of elasticity of chiral materials for Lipschitz domains, *Math. Methods Appl. Sci.* 29 (2006) 445–478.
- [18] K. Chandraseker, S. Mukherjee, Coupling of extension and twist in single-walled carbon nanotubes, *J. Appl. Mech.* 73 (2006) 315–326.
- [19] D. Ieşan, Chiral effects in uniformly loaded rods, *J. Mech. Phys. Solids* 58 (2010) 1272–1285.
- [20] R. Lakes, H.S. Yoon, J.L. Katz, Slow compressional wave propagation in wet human and bovine cortical bone, *Science* 220 (1983) 513–515.
- [21] A. Lakhtakia, V.V. Varadan, V.K. Varadan, Elastic wave propagation in non-centrosymmetric isotropic media: dispersion and field equations, *J. Appl. Phys.* 63 (1988) 5246–5250.
- [22] X.N. Liu, G.L. Huang, G.K. Hu, Chiral effect in plane isotropic micropolar elasticity and its application to chiral lattices, *J. Mech. Phys. Solids* 60 (2012) 1907–1921.
- [23] Y. Chen, X.N. Liu, G.K. Hu, Q.P. Sun, Q.S. Zheng, Micropolar continuum modeling of bi-dimensional tetrachiral lattices, *Proc. R. Soc. A* 470 (2014) 20130734.